JTTEE5 17:966–973
DOI: 10.1007/s11666-008-9272-3
1059-9630/$19.00 © ASM International

Peer Reviewed

Particle Behavior During the Arc Spraying Process with Cored Wires

W. Tillmann, E. Vogli, M. Abdulgader, M. Gurris, D. Kuzmin, and S. Turek

(Submitted May 8, 2008; in revised form September 29, 2008)

To use the manifold possibilities that arc spraying offers to deposit wear resistance layers, knowledge of the particle formation and their behavior is necessary. This work is focused on studying the particle properties during arc spraying with cored wires. Different cored wires under various spraying parameters are investigated by means of a high speed camera. Particle properties in-flight, such as velocity and temperature, are determined. Correlation between particle behavior and particle characteristics at different spraying conditions is established. At the same time, the particle-laden gas flow is simulated numerically and the computed solutions are used to illustrate the utility of the proposed CFD model and compared with experimental results. The employed mathematical model represents a system of macroscopic conservation laws for the continuous gas phase and for the gas-solid mixture. This approach formulation makes it possible to circumvent the numerical difficulties associated with the implementation of a (potentially ill-posed) two-fluid model. The discretization in space is performed using a high-resolution finite element scheme based on algebraic flux correction in terms of local characteristic variables. The artificial diffusion operator is constructed on the discrete level and fitted to the local solution behavior using a multidimensional flux limiter of TVD type.

Keywords arc spraying, CFD model, cored wires, multiphase flow, particle properties

1. Introduction

The *t*win *w*ire *a*rc *s*praying (TWAS) technique is regarded as a versatile spraying process, where the materials to be sprayed in wire form are melted (Ref 1). The melted materials are atomized and accelerated toward the substrate by means of pressurized air. The coating properties are considered to be a sum of the process parameters, which directly or indirectly influence the particle formation, size, velocity, and temperature (Ref 2, 3). Lampann (Ref 4) found out by spraying metallic wires through TWAS that particle formation is strongly affected by the atomization gas pressure. By applying a low atomization gas pressure (<2 bars), thread-shaped particles are predominantly generated. With the increase of atomization gas pressure the molten wire materials are directly atomized at the electrode spikes. The generated primary particles will further atomize under the influence of the high atomization gas pressure and the turbulent

W. Tillmann, E. Vogli, and **M. Abdulgader**, Institute of Materials Engineering, Dortmund University of Technology, Leonhard-Euler-Str. 2, 44227 Dortmund, Germany; and **M. Gurris**, **D. Kuzmin,** and **S. Turek**, Insitute of Applied Mathematics, Dortmund University of Technology, Vogelpothsweg 87, 44227 Dortmund, Germany. Contact e-mail: wolfgang.tillmann@udo.edu.

Nomenclature

Latin Alphabet

$\overline{u}_g$	Velocity of the inviscid gas, m/s
P_g	Pressure of the inviscid gas, Mpa
E_g	Total energy of the inviscid gas per unit volume, J/m^3
$\overline{u}_g$	Velocity of the disperse particle phase, m/s
E_p	Total energy of the disperse particle phase per unit volume, J/m^3
E	Energy of the mixture per unit volume, J/m^3
I	Unit tensor
M	Mach number

Greek Symbols

α_g	Volume fraction of the inviscid gas
ρ_g	Density of the inviscid gas, kg/m^3
γ_D	Rate of interphase momentum transfer, kg/(s·m^3)
α_p	Volume fraction of the disperse particle phase
ρ_p	Density of the disperse particle phase, kg/m^3
ρ	Effective density of the mixture, kg/m^3
∇	Del operator

Abbreviations

TWAS	Twin wire arc spraying
TVD	Total variation diminishing
CFD	Computational fluid dynamics
PDE	Partial differential equation
CCD	Charge-coupled device
SEM	Scanning electron microscopy

stream in so-called secondary particles, which are smaller in size than the primary particles. Thus, the particle size distribution exhibits a broad spectrum associated with an inhomogeneous coating morphology. Wen et al. (Ref 5), Watanabe et al. (Ref 6), and Hussary et al. (Ref 7) came to the same conclusion.

Recently, the use of cored wires has extended the field of TWAS application. The inhomogeneous composition of the cored wires causes an additional uncertainty in particle formation and characteristic features of particles in flight (Ref 8, 9). To have a good coating quality produced by means of cored wires and to secure the reproducibility of a desired coating, an accurate interpretation of the particle formation and particles in-flight characteristics is needed.

In addition to process and coatings characterization, effort has been made to describe the spraying processes by mathematical models (Ref 10, 11). For example, the flow behavior in a plasma torch and plasma flow after powder feeding in a plasma spraying process are described with multiphase compressible flow models, while the particle broadening and solidification as well as the determination of their size and form are characterized by employing the incompressible Navier-Stokes equations. Kamnis et al. (Ref 12) developed mathematical models to predict particle dynamic behavior in a liquid fuel high velocity oxy-fuel thermal spray gun. They applied a 3-dimensional CFD model, which employed a Lagrangian particle tracking frame coupled with a steady-state gas flow field.

In this work, an online diagnostic of particles was utilized to measure their velocity and temperature along the spray jet. The particle sizes were examined by analyzing sprayed particles, which are quenched in water during flying. In addition to the experimental work, a mathematical model was developed and applied to the TWAS process. Because of the by principal measurement restrictions, the behavior of the particles, especially the velocity, cannot be measured at a standoff distance of less then four centimeters of the nozzle exit (Ref 13). On the other hand this area is very important to understand the spray generation. Due to this fact, a computational model is developed to predict the properties of the gas and the particulate phase. Moreover, the gas properties inside the nozzle and the influence of the injected particles are rather unknown and difficult to measure. Such properties are also predicted by the proposed model. Furthermore, the physical processes controlling the TWAS are complex due to the turbulent fluid flow as well as the unsteady arcs formed between the wire tips. Modeling the process is therefore difficult and requires extensive validation. Finally, this model may help in the future to optimize the geometry and shape of the nozzle, which would require a very huge amount of work to be done by experiments. In contrast to (Ref 12), the mathematical modeling used in the present work was based on a Euler/Euler approach. The theoretical and experimental results were compared and aligned for further optimization of the mathematical model.

2. Experimental Setup

2.1 Mathematical Model

Mathematical models of particle-laden gas flows are usually based on macroscopic conservation laws that can be postulated or derived using a suitable averaging procedure (Ref 14-18). Neglecting molecular diffusion one obtains a set of partial differential equations for the mass, momentum, and energy of the continuous gas phase:

$$\partial_t(\alpha_g \rho_g) + \nabla \cdot (\alpha_g \rho_g \overline{u}_g) = 0 \quad \text{(Eq 1)}$$

$$\partial_t(\alpha_g \rho_g \overline{u}_g) + \nabla \cdot (\alpha_g \rho_g \overline{u}_g \otimes \overline{u}_g + \alpha_g P_g I) = \gamma_D \alpha_p (\overline{u}_p - \overline{u}_g) \quad \text{(Eq 2)}$$

$$\partial_t(\alpha_g \rho_g E_g) + \nabla \cdot (\alpha_g \overline{u}_g (\rho_g E_g + P_g) = \gamma_D \alpha_p \overline{u}_p (\overline{u}_p - \overline{u}_g) \quad \text{(Eq 3)}$$

where α_g, ρ_g, $\overline{u}_g$, P_g, and E_g are the volume fraction, density, velocity, pressure, and total energy of the inviscid gas. The constant coefficient γ_D denotes the rate of interphase momentum transfer due to the viscous drag force and includes information about the particles diameter (Ref 16). For simplicity, all other forces (virtual mass and lift) as well as mass and heat transfer effects are neglected. A similar system of conservation laws can be formulated for the disperse particle phase (index p):

$$\partial_t(\alpha_p \rho_p) + \nabla \cdot (\alpha_p \rho_p \overline{u}_p) = 0 \quad \text{(Eq 4)}$$

$$\partial_t(\alpha_p \rho_p \overline{u}_p) + \nabla \cdot (\alpha_p \rho_p \overline{u}_p \otimes \overline{u}_p + \alpha_p P_g I) = \gamma_D \alpha_p (\overline{u}_g - \overline{u}_p) \quad \text{(Eq 5)}$$

$$\partial_t(\alpha_p \rho_p E_p) + \nabla \cdot (\alpha_p \overline{u}_p (\rho_p E_p + P_g) = \gamma_D \alpha_p \overline{u}_p (\overline{u}_g - \overline{u}_p) \quad \text{(Eq 6)}$$

It is commonly assumed that the pressure P_g is the same for both phases and satisfies the equation of state:

$$P_g = (\gamma - 1)\rho_g \left(E_g - \frac{|\overline{u}_g|^2}{2} \right) \quad \text{(Eq 7)}$$

Furthermore, the volume fractions of the continuous and disperse phase are coupled by the constraint:

$$\alpha_g + \alpha_p \equiv 1 \quad \text{(Eq 8)}$$

Inviscid two-fluid models such as (1)-(6) are particularly difficult to solve numerically due to the lack of hyperbolicity and uncertainty regarding the modeling of the disperse phase in particle-free regions. If the volume fraction of particles equals zero, the effective density $\alpha_p \rho_p$ and momentum $\alpha_g \rho_g \overline{u}_g$ show the same behavior. As a consequence, the velocity of particles $\overline{u}_p$ is not uniquely defined, which may give rise to nonphysical solutions and waves moving at wrong speeds. Clearly, such a potentially degenerated two-fluid model is of little practical utility. To circumvent the above mathematical and numerical difficulties, the gasparticle mixture was considered as a single

fluid. The effective density, momentum, and energy of the mixture are given by the following equations:

$$\rho = \alpha_p \rho_p + \alpha_g \rho_g \quad \text{(Eq 9)}$$

$$\rho \overline{u} = \alpha_p \rho_p \overline{u}_p + \alpha_g \rho_g \overline{u}_g \quad \text{(Eq 10)}$$

$$\rho E = \alpha_p \rho_p E_p + \alpha_g \rho_g E_g \quad \text{(Eq 11)}$$

The so-defined conservative variables ρ, $\rho\overline{u}$, and ρE are assumed to satisfy the compressible Euler equations:

$$\partial_t(\rho) + \nabla \cdot (\rho \overline{u}) = 0 \quad \text{(Eq 12)}$$

$$\partial_t(\rho \overline{u}) + \nabla \cdot (\rho \overline{u} \otimes \overline{u} + P_g I) = 0 \quad \text{(Eq 13)}$$

$$\partial_t(\rho E) + \nabla \cdot (\overline{u}(\rho E + P_g) = 0 \quad \text{(Eq 14)}$$

By definition of the mixture density ρ, the continuity Eq 12 is the sum of (1) and (4). The effective pressure of the mixture can also be defined as P_g plus a correction describing the influence of the particles (Ref 19, 20).

The derivation of drift-flux/mixture models can be found in (Ref 21) among others. The model used in the present work does not incorporate turbulence explicitly. The modeling of turbulence phenomena is rather controversial especially in the framework of multiphase flow. Moreover, turbulence modeling results in overdiffusive schemes due to the additional turbulent diffusion and increases the computational complexity. On the other hand, the numerical diffusion, which is added by the nonlinear high-resolution scheme, can be viewed as an implicit large eddy simulation. Therefore, many researchers shift their focus to the implicit modeling of turbulence, provided by the nonlinear discretization scheme (Ref 22). The implicit treatment of turbulence is adopted in this study as well.

In the present work, Eq. 12 to 14 are solved instead of (1)-(6), whereby the density, momentum, and energy of the particulate phase can be readily inferred from algebraic relations (9)-(11). This formulation can be classified as a drift-flux model. The PDE system to be solved consists of subproblems (1)-(3) and (12)-(14) both of which reduce to the Euler equations of gas dynamics in particle-free regions, where the standard two-fluid model (1)-(6) is not applicable.

2.2 Spraying Experiments

To study the particle behaviors by arc spraying, a device with a closed nozzle system Smart Arc 350 PPG (Sulzer Metco, Switzerland) was used. As feedstock a Fe-based cared wise and a Ni-based cored wire with a diameter of 1.6 mm and hard particle grain size of 40-70 μm were employed (Fig. 1). The composition of the used cored wires is shown in Table 1 and the experimental setup is shown in Fig. 2.

In an aim to analyze the particles formation as well as their temperature and velocity along the spray jet, the standoff distance was varied between 45 and 150 mm, while other spraying parameters were kept constant (Table 2). The electric current and voltage levels were taken from prior works, in which the arc ignition stability and arc fluctuations were analyzed (Ref 23).

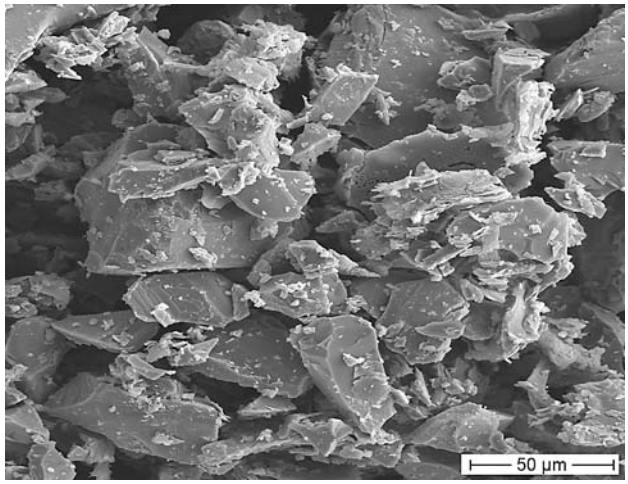

Fig. 1 SE micrograph of hard particles in Fe-based cored wire

Table 1 Composition of the employed wires

Wire	Content, wt.%	Grain size, μm	Velum material	Velum thickness, μm
FeCrBSiMn	Cr-29; Mn-1,6; Si-1,6; B-3,8; Fe-Bal.	40-70	Fe	200
NiCrBSi+PC	Cr-24; Si-5,25; B-1,8; PC-0,4; Ni-Bal.	40-70	Ni	200

The particle temperature and velocity at different standoff distances were measured by means of Accuraspray-g3 (Tecnar, Canada). The properties are measured within two measuring volumes with a dimension of 3 mm in diameter and 25 mm in length. Through a dual fiber optical system the flow of particles at two different points along the spray jet were detected, and the velocity is determined as a ratio of the gap between two measuring points and the time delay. Based on the twin wave length pyrometer principle, the mean particle temperature is measured. In this case, it was assumed that the emissivity of the particles is the same for the two wave lengths.

The particle formation and atomization were analyzed by means of a high speed camera (PCO, Germany), which is equipped with a TV-zoom lens with a 0.9× to 6.3× magnification (Opto Sonderbedarf GmbH, Germany). This camera system comprises an image splitter unit, four intensified CCD camera modules with fast switchable MCP image intensifiers, and high-resolution CCD image sensors. Each module with its 12 bit dynamic range and a high-resolution CCD image sensor features a good signal-to-noise-ratio and the ability of single photon detection. Four high speed serial fiber optic data links connect the system to a PC. All images in this study have been captured at a framing rate of 333 megaframes/s with an image resolution of 1280 × 1024 pixels. To investigate the particle size during arc spraying experiments, a custom-made

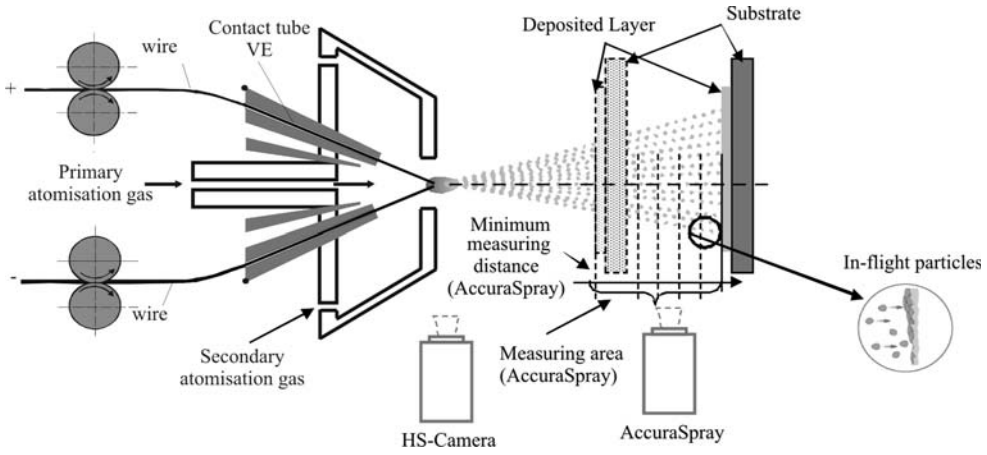

Fig. 2 Experimental setup

Table 2 Arc spraying process parameters

Parameter	Parameter value
Current, A	320
Voltage, V	32
Primary air pressure, bar	6
Secondary air pressure, bar	0
Spraying distance, mm	45-150

experimental setup was designed and applied (for more details, see Ref 23). The generated particles were analyzed by means of SEM (SEM, JSM-840, Co. Jeol, Japan) with respect to their size and shape. Correlation between particle sizes, their temperatures, and velocities were studied. Finally, the results from the mathematical model were compared to the experimental results.

3. Results and Discussion

3.1 Numerical Algorithm and Results

The numerical treatment of coupled PDE systems that constitute an inviscid two-fluid/drift-flux model is a very challenging task. Most of the numerical algorithms published to date are based on a finite difference or finite volume discretization, while the use of finite elements is rather uncommon in this area of CFD research.

Our implementation of the new drift-flux model (1)-(3), (12)-(14) is based on a high-resolution finite element scheme, which is applicable to unstructured meshes and implicit time-stepping schemes. A multidimensional generalization of Roe's approximate Riemann solver and an algebraic flux correction scheme of TVD type are constructed building on the methodology described in (Ref 24-26). The design of the artificial viscosity operator, flux limiting, and artificial implementation of the numerical boundary conditions are performed in terms of local characteristic variables. Particle-laden jets may give rise to low Mach number regions that coexist with sonic points and local supersonic regions. The stiffness associated with the wide range of Mach numbers to be resolved calls for the use of an unconditionally stable implicit time discretization. Explicit schemes turn out rather inefficient, unless characteristic time stepping or local preconditioning is employed. The stationary counterpart of the above drift-flux model is solved using the fully implicit backward Euler method to match the solution to a steady state. This pseudo-time-stepping scheme can be interpreted as an iterative solver, whereby the artificial time step serves as a variable under relaxation parameter.

The validation of the proposed drift-flux model in the context of thermal spraying processes is complicated by the lack of experimental data and reliable benchmarks for this class of multiphase flows. The numerical results for a prototypical 2D configuration with a simplified nozzle are depicted in Fig. 3.

The simplified nozzle consists of two wires, which are modeled by solid walls with a gas-particle inlet in-between. Since no model of particle formation and atomization is available so far, the particles are injected through the boundary in the vicinity of the wires. The volume fraction of particles equals $\alpha_p = 0.001$ at the inlet. The dimensions of the computational domain are 0.1 m × 0.1 m. Numerical solutions are computed on an unstructured triangular mesh with 48,785 nodes and a total of 390,280 unknowns.

The presented simulation results were computed using the supersonic boundary conditions:

$$M_g = 1.1,\ P_g = 0.2\,\text{MPa},\ u_{1P} = u_{1g}$$

$$u_{2g} = u_2 = 0\,\text{m/s},\ \rho_g = 2.3767\,\text{kg/m}^3$$

in the region between the wires and the slip condition on the wires. The slip conditions are implemented by projecting the residual and the solution on the tangent to the boundary. At the remaining boundaries, atmospheric conditions are prescribed for the incoming Riemann invariants. The density of the particles (nickel) is $\rho_p = 8908\ \text{kg/m}^3$ and the viscous drag is given by $\gamma_D = 1.26 \times 10^6\ \text{kg/(s m}^3)$. At the postprocessing step, it is assumed that the particles move with the gas velocity if the

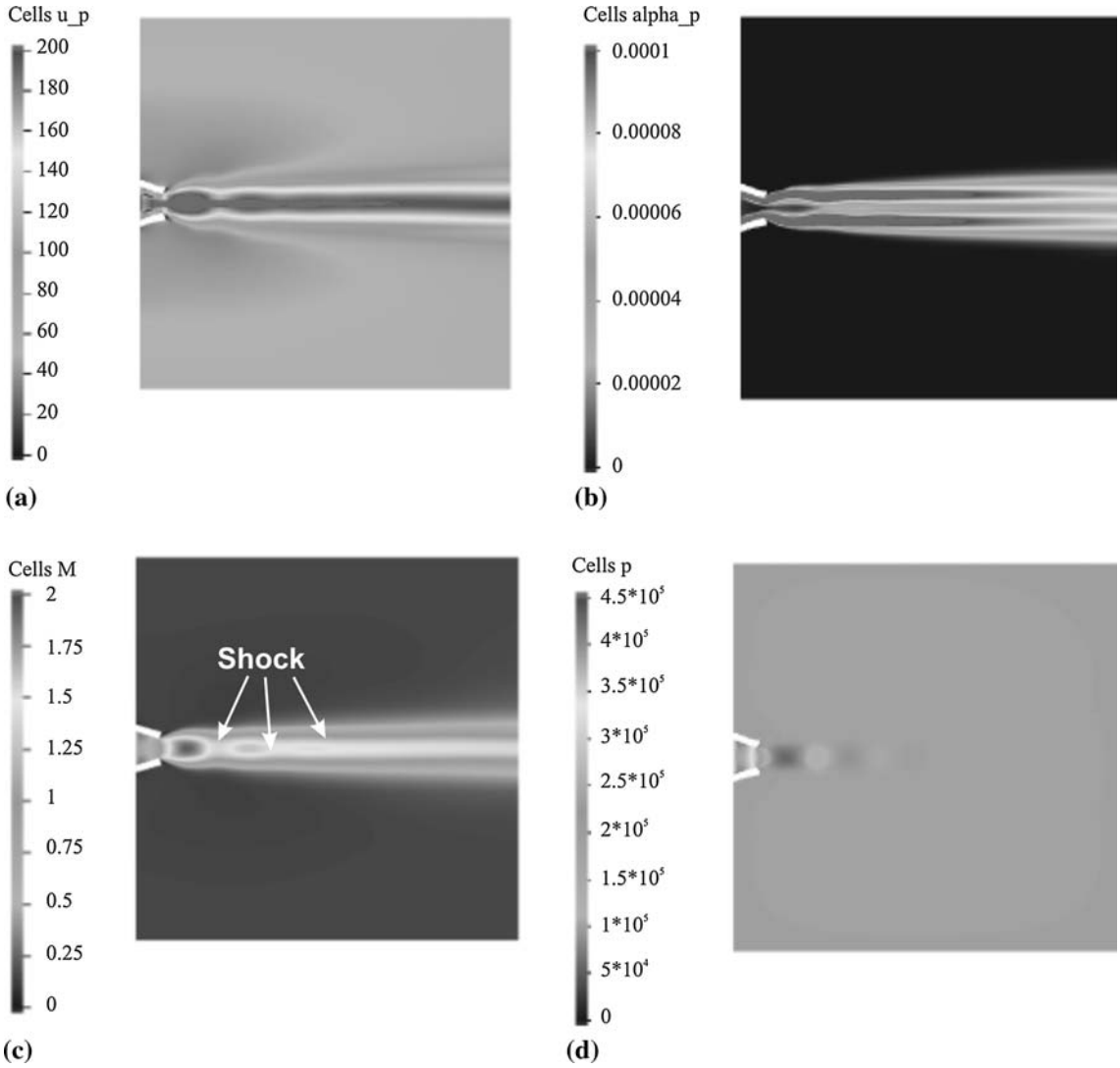

Fig. 3 Numerical results of (a) particle velocity in m/s; (b) volume fraction of particles in %; (c) Mach number of the gas; and (d) gas pressure in Pa

volume fraction is less than 10^{-7}. This prevents division by zero and does not affect the computed solution.

Due to the lack of experimental measurements of the gas inlet data and the particle mass flux at the current state, these quantities are only estimated for the computations. This leads to an overestimation of the velocities and the Mach number. Therefore, more accurate estimates of the inlet boundary conditions will give more accurate velocities. Note that these overestimations arise from the estimation of the boundary values and they are not caused by the computational model.

On the other hand, these results compare qualitatively well with the ones computed by Pourmousa (Ref 27). Especially the pressure profile at a standoff distance of more than five centimetres is approximately the same. This indicates an accurate prediction of the pressure by this model, which is an important issue in multiphase flow modeling. Furthermore the velocities decrease in a short standoff distance in front of the nozzle, remain rather constant near the outlet boundary (see Ref 27), and depend on the pressure (a high gas pressure results in a high particle velocity and vice versa Ref 7). Moreover, three shocks with a very high Mach number at a standoff distance of about 18, 35, and 50 mm in front of the nozzle are observed. These high Mach number regions cause the turbulences, which are observed in the experimental results. Wilden comes to the same conclusion (Ref 28). Taking everything into consideration, this model is able to predict the main properties of arc spraying, which are also observed by other researchers. To improve the results, more accurate estimates of the inlet boundary conditions are necessary.

3.2 Spraying Results

The results of particle velocities along the spray jet for both kinds of wires employed are shown in the Fig. 4. Particles generated from both wires exhibit the same

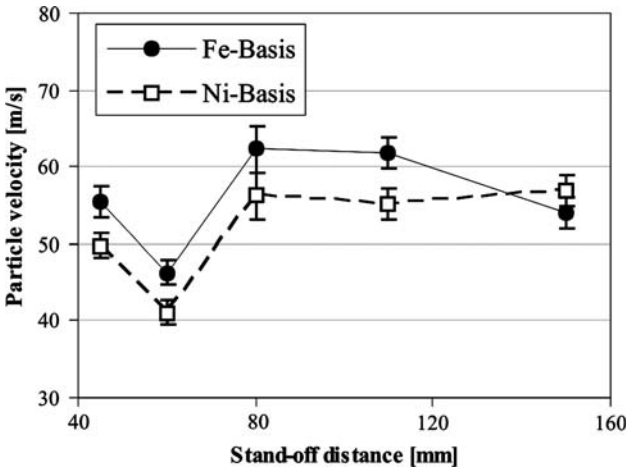

Fig. 4 Variation of particle velocity along the spray jet

behavior. The velocity of particles decreases up to a standoff distance of 60 mm. This is in accordance with the mathematical modeling results. At a standoff distance of 50 mm a shock wave is predicted in the mathematical model, which is associated with turbulences (see Fig. 3d). Due to the high gas pressure of the spray jet and the existing turbulences in this area, the particles are decelerated and therefore have low velocities. No turbulences were predicted in the mathematical model at standoff distances larger than 50 mm, which is verified in experimental measurements. The particle velocities posses approximately a constant value after a standoff distance of 80 mm.

It is worth nothing that the particles generated from Fe-based wires possess higher velocities than the particles generated from Ni-based wires (Fig. 4). To explain this different behavior the particles generated from both wires during spraying were analyzed by means of SEM (Fig. 5). The Fe-based particles show a mean particle size of 6 μm (Fig. 5a), while the mean particle size of Ni-based particles is 8.4 μm (Fig. 5b). The different particle sizes are explained with different melting points of the wires velum. Ni-based wires have a Ni-velum with a melting point at 1455 °C, while the Fe-based wires have a Fe-velum with a melting point at 1538 °C (Ref 29). Therefore by applying the same spraying parameter (voltage and current) the melting rate of Ni-based wires is larger than that of the Fe-based wires. Consequently, more material is molten on Ni-based wire tips than on Fe-based wire tips. This is associated with a higher atomization rate of Fe-based melting bath and smaller particle sizes compared to Ni-based wires during continuous removal of generated melted bath from the wire tips. Hussary and Heberlein (Ref 7) also came to the same conclusion by arc spraying of steel wires.

The turbulences developed in the spray jet favour in turn the atomization process of generated particles as a result of aerodynamic forces. By analyzing the arc jet with the high speed camera, it was found that after the first atomization of the melting bath large particles are

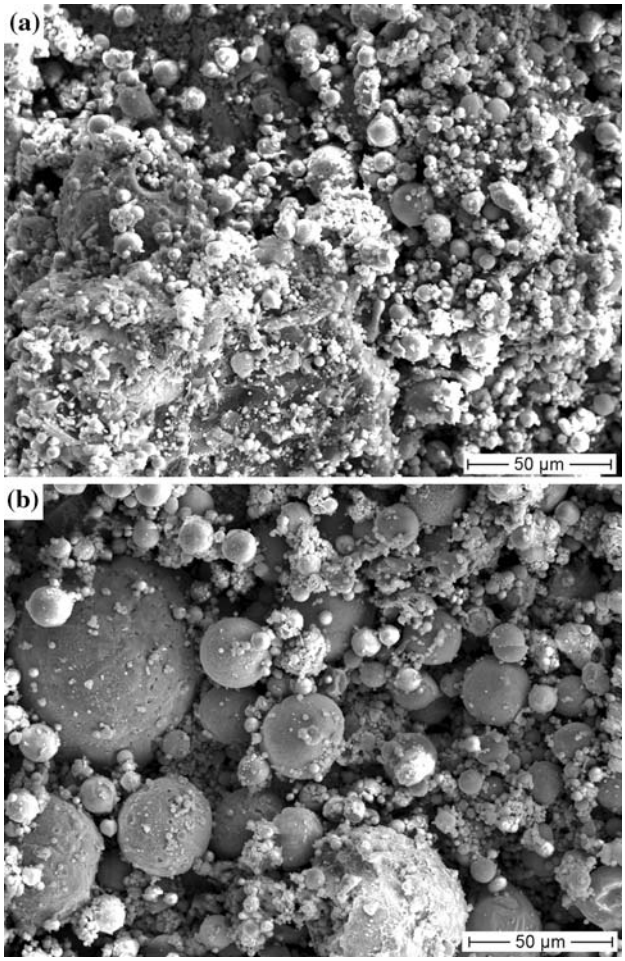

Fig. 5 SE micrographs of (a) Fe- and (b) Ni-based particles

produced (Fig. 6). Along the spray jet they are fragmented in to smaller particles. Hussary and Heberlein (Ref 7) and Newbery et al. (Ref 30) came to the same conclusion by studying arc spraying of metallic wires and spraying of steel wires, respectively. They explain this behavior with the aerodynamic forces and breakup mechanisms of molten bath.

After atomization, particles with smaller sizes are produced, which move with higher velocities than the larger particles at the same gas pressure levels. This explains the higher velocities of small Fe-based particles compared to the large Ni-based particles.

However, the movement of particles in the spray jet depends on the spray jet properties. At high turbulences (high Mach and Reynolds number), the small particles can be more easily stopped during flight due to their low weight, which explains the slight decrease of the velocities of the Fe-based particles at 150 mm standoff distance Mahesh et al. (Ref 31) came to the same conclusion by modeling and analyzing droplet dynamic and thermal behavior of particles during thermal spray deposition. They found out that the smaller particles attain maximum velocity at a shorter time, and subsequently they travel

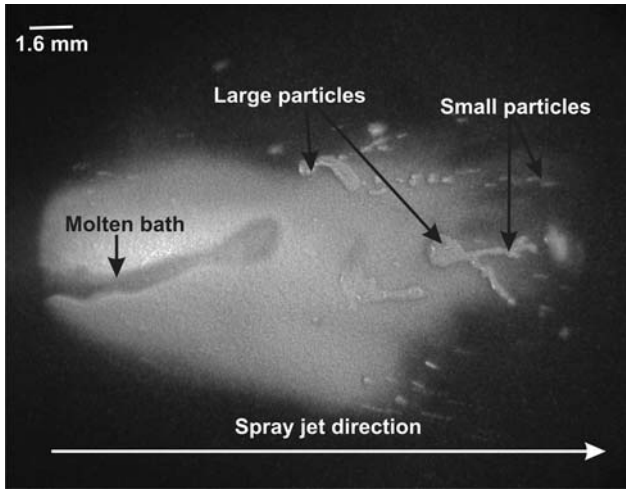

Fig. 6 High speed camera image of Fe-based wire

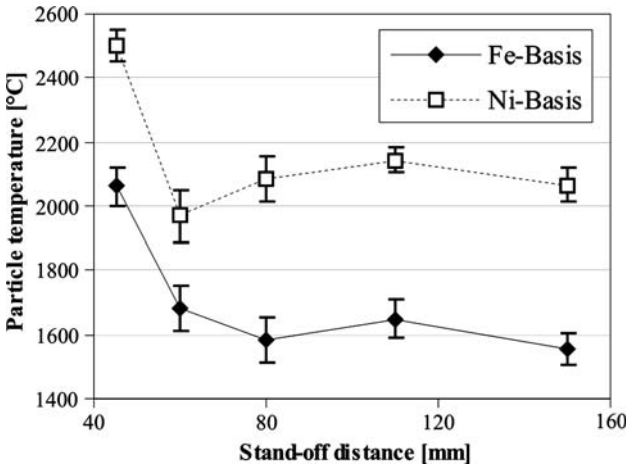

Fig. 7 Variation of particle temperature along the spray jet

faster after atomization than the larger particles. On the other hand the drag forces of small particles are increased during flight within the spray jet, and as a result small particles are decelerated. On the contrary, the drag coefficient for the large particles is low and approximately constant and therefore they do not show a significant deceleration during flight. Watanabe et al. (Ref 32) came to the same conclusion by spraying Ti-Al intermetallic compounds via TWAS process.

The temperature of the particles shows a decrease of approximately 26% with the standoff distance independent of the kind of wires (Fig. 7). The atomization gas and the environmental air impose a cooling effect on the accelerated particles. The smaller the particles, are the larger the contact area with the gas is, which leads to a higher heat transfer. Therefore, the Ni-based particles with larger sizes feature higher temperatures than the Fe-based particles Mahesh et al. (Ref 31) came to the same conclusion by studying Al-Si-Mg-alloy spraying.

4. Conclusions

A new mathematical model of Euler-Euler type was presented for the process of arc spraying. This model represents a generalization of the compressible Euler equations to particle-laden gas flows. Unlike the usual two-fluid model, the equations to be solved remain valid in particle-free regions. Promising results were obtained for a simplified 2D model problem. Further research is required to improve the robustness and efficiency of the numerical algorithm. Work is under way to impose characteristic boundary conditions in a weak sense and accelerate convergence to the steady state using a nonlinear multigrid solver. Furthermore, an Euler-Lagrange model of particulate flow is to be implemented for validation purposes.

Experimental results show a deceleration of particles up to a stand off distance of 60 mm due to the turbulences in this area. This is also associated with a further atomization of particles. It is also found that the higher the wires melting point is, the less the material melts, and smaller particles are generated. Due to the high surface area of smaller particles compared to the larger particles, the smaller particles cool down along the spray jet faster than the larger particles. Further analyses and measurements must be conducted at different pressure levels, voltages, and electric currents to explain the melting behavior and breakup mechanisms of cored wires during arc spraying.

Acknowledgments

The authors gratefully acknowledge the financial support of the DFG (German Science Foundation) within the Collaborative Research Centre SFB 708.

References

1. Fr.-W. Bach, K. Möhwald, A. Laarmann, and Th. Wenz, *Modern Surface Technologies*, Wiley-VCH Verlag, Germany, 2005, p 370
2. J. Wilden, A. Wank, and F. Schreiber, Wires for Rrc- and High Velocity Flame Spraying—Wire Design, Materials and Coatings Properties, *Thermal Spray: Surface Engineering via Applied Research*, C.C. Berndt, Ed., May 8-11, 2000 (Montréal, Québec, Canada), ASM International, Materials Park, OH, USA, 2000, p 609-617
3. M. Nakagawa, K. Shimoda, T. Tomoda, M. Koyama, Y. Ishikawa, and T. Nakajima, Development of Mass Production Technology of Arc Spraying for Automotive Engine Aluminum Alloy Valve Lifters, *Thermal Spray Research and Applications*, T.F. Bernecki, Ed., May 20-25, 1990 (Long Beach, California), ASM International, Materials Park, OH, USA, 1991, p 457-464
4. F. Lampmann, Entwicklung einer Hybridbeschichtungstechnologie zur Herstellung von Hochleistungs-Diesel-Pleuellagern, Dissertation TU Berlin, 2005, 187 p (in German)
5. J. Wen and S. Wen, Aerodynamic Behavior Within the Arc Gap During Arc Spraying, *Thermal Spray Industrial Applications*, C.C. Berndt and S. Sampath, Eds., June 20-24, 1994 (Boston, MA), ASM International, Materials Park, OH, USA, 1994
6. T. Watanabe, X. Wang, E. Pfender, and J. Heberlein, Correlations Between Electrode Phenomena and Coating Properties in Wire Arc Spraying, *Thin Solid Films*, 1998, **316**, p 169-173

7. N. Hussary and J. Heberlein, Metal Droplet Formation Mechanisms in the Wire Arc Spraying Process, *Proc. 48th International Research Colloquium* (Illmenau, Germany), Sept 22-25, 2003
8. M.P. Planche, H. Liao, and C. Coddet, Relations Between In-Flight Particle Characteristics and Coating Microstructure with a Twin Wire Arc Spray Process and Different Working Conditions, *Surf. Coat. Technol*, 2004, **182**, p 215-226
9. F. Schreiber, Karbidische Werkstoffe zum Thermischen Spritzen, http://www.durmat.com/PDF-Files/d_Karbidische_Werkstoffe.pdf, DURUM-VERSCHLEISS-SCHUTZ GMBH, Willich (in German)
10. H.H. Tawfik and F. Zimmerman, Mathematical Modelling of the Gas and Powder Flow in HVOF Systems, *J. Thermal Spray Technol.*, 1997, **6**(3), p 345-252
11. H. Hu and S.A. Argyropoulos, Mathematical Modelling of Solidification and Melting: A Review, *Model. Simul. Mater. Sci. Eng.*, 1996, **4**(4), p 371-396
12. S. Kamnis, S. Gu, and N. Zeoli, Mathematical Modeling of Inconel 718 Particles in HVOF Thermal Spraying, *Surf. Coat. Technol.*, 2008, **202**(12), p 2715-2724
13. http://www.tecnar.com/DATA/DOCUMENT/Accuraspray-g3%20Reference%20Manual.pdf
14. H. Städke, *Gas Dynamic Aspects of Two-Phase Flow*, Wiley-VCH, 2006, 450 p
15. D. Drew, Mathematical Modeling of Two-Phase Flow, *Annu. Rev. Fluid Mech.*, 1983, **15**, p 261-291
16. C.E. Brennen, *Fundamentals of Multiphase Flows*, Cambridge University Press, 2005, 342 p
17. M. Pelanti and R.J. Leveque, High-Resolution Finite Volume Methods for Dusty Gas Jets and Plumes, *SIAM J. Sci. Comp.*, 2006, **28**(4), p 1335-1360
18. T. Flatten and S.T. Munkejord, The Approximate Riemann Solver of Roe Applied to a Drift-Flux Two-Phase Flow Model, *ESAIM*, 2006, **40**(4), p 735-764
19. F.H. Harlow and A.A. Amsden, Numerical Calculation of Multiphase Fluid Flow, *J. Comput. Phys.*, 1975, **17**, p 19-52
20. T. Saito, Numerical Analysis of Dusty Gas Flows, *J. Comput. Phys.*, 2002, **176**, p 129-144
21. M. Manninnen and V. Taivassalo, On the mixture model for multiphase flow, *VTT Publications 288*, Technical Research Centre of Finnland, 1996
22. F.F. Grinstein and C. Fureby, On Monotonically Integrated Large Eddy Simulation of Turbulent Flows Based on FCT Algorithms. *Flux Corrected Transprot: Principles, Algorithms and Applications*, D. Kuzmin, R. Lohner, and S. Turek, Eds., Springer, Germany, 2005, p 79-130
23. W. Tillmann, E. Vogli and M. Abdulgader, Influence of Atomisation Gas on the Particle Formation During Arc Spraying with Cored Wires, *Thermal Spray 2007, Global Coating Solutions*, B.R. Marple, M.M. Hyland, Y.-C. Lau, C.-J. Li, R.S. Lima and G. Montavon, Eds., ASM International, Materials Park, Ohio/USA, 2007, p 837-842
24. D. Kuzmin and M. Möller, Algebraic Flux Correction I. Scalar Conservation Laws. *Flux-Corrected Transport: Principles, Algorithms, and Applications*, D. Kuzmin, R. Lohner, and S. Turek, Eds., Springer, Germany, 2005, p 155-206
25. D. Kuzmin and M. Möller, Algebraic Flux Correction II. Compressible Euler Equations. *Flux-Corrected Transport: Principles, Algorithms, and Applications*, D. Kuzmin, R. Löhner, and S. Turek, Eds., Springer, Germany, 2005, p 207-250
26. D. Kuzmin, Algebraic Flux Correction for Finite Element Discretizations of Coupled Systems. *Computational Methods for Coupled Problems in Science and Engineering II*, E. Önate, M. Papadrakakis, and B. Schrefler, Eds., CIMNE, Barcelona, 2007, p 653-656
27. A. Pormousa, ''Wire-Arc Spraying System: Particle Production, Transport and Deposition,'' Dissertation, University of Toronto, 2007, 148 p
28. J. Wilden, Virtuelles Werkstoff- und Prozessdesign funktioneller Schichten, *Mat.-wiss. u. Werkstofftech.*, 2007, **38**(2), p 131-138 (in German)
29. http://nt-systemloesungen.de/index.php?opt-ion=com_content&task=view&id=209&Itemid=171.N.S
30. A.P. Newbery, P.S. Grant, and T.R.A. Neiser, The Velocity and Temperature of Steel Droplets During Electric Arc Spraying, *Surf. Coat. Technol.*, 2005, **195**, p 91-101
31. M.J. Mendonca, M.K. Muralidhara, B.K. Muralidhara, and C. Ramachandra, Modeling of Droplet Dynamic and Thermal Behaviour During Spray Deposition, *Bull. Mater. Sci.*, 2003, **26**(3), p 355-364
32. T. Watanabe, T. Sato, and A. Nezu, Electrode Phenomena Investigation of Wire Arc Spraying for Preparation of Ti-Al Intermetallic Compounds, *Thin Solid Films*, 2002, **407**, p 98-103